ACS APPLIED MATERIALS & INTERFACES

Research Article

www.acsami.org

Verification of Icephobic/Anti-icing Properties of a Superhydrophobic Surface

Yuanyi Wang,[†] Jian Xue,[†] Qingjun Wang,[†] Qingmin Chen,*[,†] and Jianfu Ding[‡]

[†]Polymer Science and Engineering Department, School of Chemistry and Chemical Engineering, State Key Laboratory of Coordination Chemistry, Nanjing University, Nanjing, Jiangsu 210093, China

[‡]Security and Disruptive Technologies, National Research Council Canada, Ottawa, Ontario K1A 0R6, Canada

Supporting Information

ABSTRACT: Four aluminum surfaces with wettability varied from superhydrophilic to superhydrophobic were prepared by combining an etching and a coating process. The surface wettability was checked in terms of water contact angle (CA) and sliding angle (SA) under different humidity at −10 °C. High-speed photography was applied to study water droplet impact dynamics on these surfaces. It was found that single and successive water droplets could rebound on the superhydrophobic surface and roll off at a tilt angle larger than 30° under an extremely condensing weather condition (−10 °C and relative humidity of 85−90%). In addition, the superhydrophobic surface showed a strong icephobic property, the ice adhesion on this surface was only 13% of that on the superhydrophilic surface, though they had a similar nano/microtopological structure. Moreover, this superhydrophobic surface displayed an excellent durability of the icephobic property. The ice adhesion only increased to 20% and 16% of that on the superhydrophobic surface after the surface was undergone 20 icing/ice-breaking cycles and 40 icing/ice-melting cycles, respectively. Surface profile and XPS studies on these surfaces indicated a minor damage of the surface nano/microstructure and the coating layer upon these multiple ice-breaking and ice-melting processes. Therefore, this superhydrophobic surface could be a good candidate for icephobic applications.

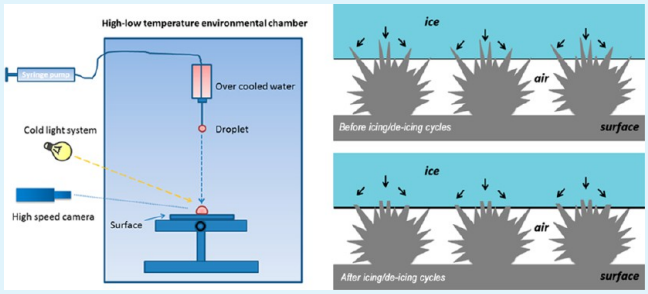

KEYWORDS: *superhydrophobic, ice-repellent, impact dynamics, ice adhesion, contact angle, sliding angle, temperature, relative humidity*

INTRODUCTION

Many flora and fauna surfaces in nature exhibit superhydrophobic and self-cleaning properties and lotus leaf is the most typical representative. The phenomenon which water droplets bead up on the surface and drip off with dust rapidly is called "lotus effect".[1] Inspired by this phenomenon, researchers have recently made significant progress in fabrication of superhydrophobic surfaces with a water contact angle (CA) greater than 150° and a sliding angle (SA) less than 10°.[2,3] One attractive application of superhydrophobic surfaces is based on their speculated icephobic or anti-ice capability.[4−6]

An ideal anti-ice surface should possess the follow two characteristics. One is that overcooled water droplets could roll off the surface rapidly before ice formation.[7] The other is that the ice adhesion should be weak when ice accumulated on the surface.[8] However, most superhydrophobic surfaces lose part or all of their superhydrophobicity under an overcooled condition, such as in the weather of freezing rain and wet snow.[9] This leads to a dramatic decrease in CA and a significant increase in SA. A surface with a SA less than 10° in an overcooled or extremely condensing environment (−10 °C, relative humidity (RH) 90%) has not been found in the literature among diversified superhydrophobic surfaces. Xiao et al.[10] found a substantial decline of CA on a nanoporous carbon superhydrophobic surface in a condensing environment (5 °C with nearly saturated humidity) for 20 min. They concluded this change was due to water condensed in the pores of the carbon nanostructure. Wier et al.[11] studied the condensation evolution on their micropillar array using an optical microscope, and observed that water droplets initially formed in the array voids, and then adjacent water droplets would consolidate, grow up and firmly anchor on the superhydrophobic surface in the end, causing the water droplet on the surface to lose mobility.

Using high speed photography to track water droplet impact dynamics on surfaces will help to figure out the interaction between surface and water droplets. Alizadeh et al.[12] presented an in-depth analysis of ice formation dynamics upon a room temperature water droplet impacting cold surfaces with different wettability. They demonstrated that ice nucleation under a low-humidity can be retarded on superhydrophobic surface since the reduction of water-surface contact area. Recently, Mishchenko et al.[7,13] showed that water droplets impinging on superhydro-

Received: January 31, 2013
Accepted: March 28, 2013
Published: March 28, 2013

   dx.doi.org/10.1021/am400429q | *ACS Appl. Mater. Interfaces* 2013, 5, 3370−3381

phobic surfaces exhibited nonicing behavior if the time scale for the droplet wetting and retracting on the surface is smaller than the ice nucleation time. However, few researches focused on the impact dynamics of overcooled water droplets under an extremely condensing condition with a low temperature and high humidity.

A survey of the recent literature indicates that researchers pay more attention on the surface ice adhesion through the exploration of superhydrophobic surface for icephobic applications. Foremost among these is the reduction of ice adhesion[14,15] and the delay of ice nucleation.[5,16,17]

Dotan et al.[18] showed that up to 18-fold reduction of ice adhesion on superhydrophobic surfaces. Kulinich et al.[6] suggested that the icephobic performance of a superhydrophobic surface declined as icing/deicing cycles proceed because of the damage of the rough surface structure, indicating that the rough surface structure was essential to icephobic property. However, the same as for superhydrophobic property, a rough surface was not a sufficient condition for icephobic property. In the case the cavities on the rough surface could be wetted by the moisture from the environment upon freezing, the condensed water in the cavities could turn to ice roots to anchor the ice layer into the rough surface structure. Thus ice adhesion would increase with surface roughness.[19] This effect can be prevented only when the surface becomes hydrophobic enough to prohibit water entering the cavity through wetting process or even condensation. Therefore the water-repellent property of a superhydrophobic surface is important for an icephobic property. This property was observed from several superhydrophobic surfaces with various chemical structures and size scales of the surface structures.[5,7,13,18] At the end, the durability of icephobicity of the surfaces was also critical factor for real applications.[6]

In this paper, four surfaces were prepared with wettability differed from superhydrophilic[20] to superhydrophobic. Their surface wettability in terms of CA and SA under different humidity at −10 °C, and the ice-repellent property of the superhydrophobic surface were studied. The ice-repellent tests included the impact dynamics of overcooled water under several environmental conditions from normal to extremely condensing (−10 °C and atmosphere relative humidity 95%). The icephobic property (reduction of ice adhesion) and its durability upon two multiple deicing (ice-breaking and ice-melting) processes were studied. It has been suggested that both binary nano/micro-surface structure and low surface tension of the surface material are essential to superhydrophobic as well as ice-repellent property (reduction in icing and ice adhesion). It is also demonstrated that the superhydrophobic surface prepared in this work has an excellent ice-repellent property for active icephobic applications.

EXPERIMENTAL SECTION

Materials. 1H,1H,2H,2H-perfluorodecyltriethoxysilane [$CF_3(CF_2)_7CH_2CH_2Si(OC_2H_5)_3$, PTES] was obtained from Fluorochem. Aluminum plates (AA1060H24, 0.5 mm thick and 26 mm in diameter) were purchased from Southwest Aluminum (China). Methanol, acetone, toluene, xylene, hydrofluoric acid (HF, 40 wt %), and hydrochloric acid (HCl, 37 wt %) were purchased from Nanjing Chemical Reagent Co. Ltd. (China). ALL these materials were used as received.

Sample Preparation. Etching solution:[21,22] A mixed acid solution was prepared by adding 2.5 mL of HF (40 wt %) and 40 mL of HCl (37 wt %) in 12.5 mL of deionized water.

Coating solution: A PTES solution was prepared by dissolving PTES (0.5 wt %) in a mixture of methanol (88 wt %), deionized water (10 wt %) and HCl (0.1 M, 1.5 wt %).

Sample 1#: The as received aluminum plates were washed with toluene, acetone and deionized water subsequently using an ultrasonic bath and then dried at room temperature (23 °C) for 24 h to obtain samples with a relatively smooth surface.

Sample 2#: The cleaned aluminum plates were coated with a cross-linked PTES layer by dipping in the PTES coating solution for four times and then cured at 100 °C for 6 h to produce samples with a PTES coated smooth surface.

Sample 3#: The cleaned aluminum plates were etched by immersing in the acid solution for 40s, followed by thoroughly cleaning in an ultrasonic bath with deionized water to remove residual acids and drying in an oven at 100 °C for 2 h to yield samples with a roughened surface.

Sample 4#: Sample 3# were coated in the same way as Sample 2# to generate samples with a PTES coated rough surface.

Characterization. A modified optical angle meter (Cam 200, KSV Instrument Ltd., Finland) was utilized to measure static contact angle (CA) and sliding angle (SA) in a microclimate chamber with a controlled humidity and temperature.[21,23,24] The environmental control system consisted of a thermostatic bath, two ultrasensitive T-type thermocouples, a nitrogen/water vapor flux, a hygro-scope and a data acquisition system. The surface temperature of the samples was precisely maintained in a range of 30 to −40 °C by the thermostatic bath, and the temperatures of the surface and in atmosphere were well controlled and recorded simultaneously. The relative humidity (RH) inside the chamber was regulated by adjusting the feeding rate of dry nitrogen and water vapor, and measured by a hygroscope with a relative error of about 3%.

The topographies and composition of the surfaces before and after the multiple icing/-deicing tests were analyzed with an Ambios XI-100 surface profiler (Ambios Technology Corp., U.S.A) with a resolution of 0.2 nm, scanning electron microscopy (SEM, Hitachi S-4800, Japan) equipped with an energy-dispersive X-ray spectrometer (EDS, Horiba Ltd., EMAX) and a X-ray photoelectron spectroscopy (XPS, PHI5000 Versa Probe, ULVAC-PHI Inc., Japan) with monochromatic Al Ka radiation. Binding energies were calibrated by setting C 1s line at 284.8 eV.

The impact experiments of overcooled water droplets were conducted using the apparatus illustrated schematically in Figure 1. A flat tip needle (0.1 mm inner diameter) was connected to a dispensing system and a 15 mL water bottle by plastic tubing. The water contacting parts of the whole system including the bottle, needle and tubing was made of polypropylene, and their inner wall was treated with the PTES solution following a same procedure as the Al surface treatment described previously to prevent ice nucleation. Fifteen mL of ultrapure

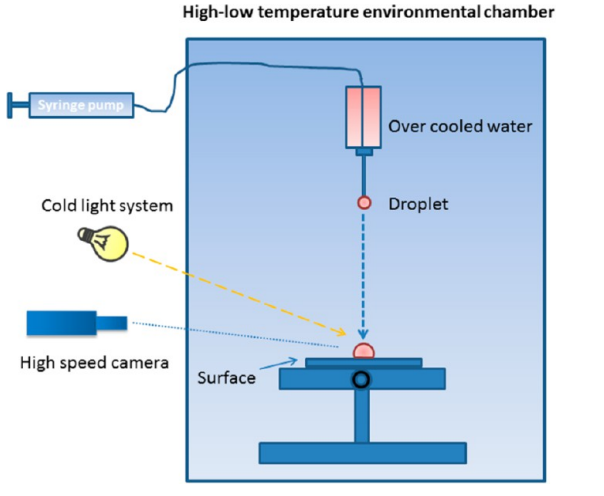

Figure 1. Schematic diagram of the impact experiment of overcooled water droplets.

dx.doi.org/10.1021/am400429q | ACS Appl. Mater. Interfaces 2013, 5, 3370−3381

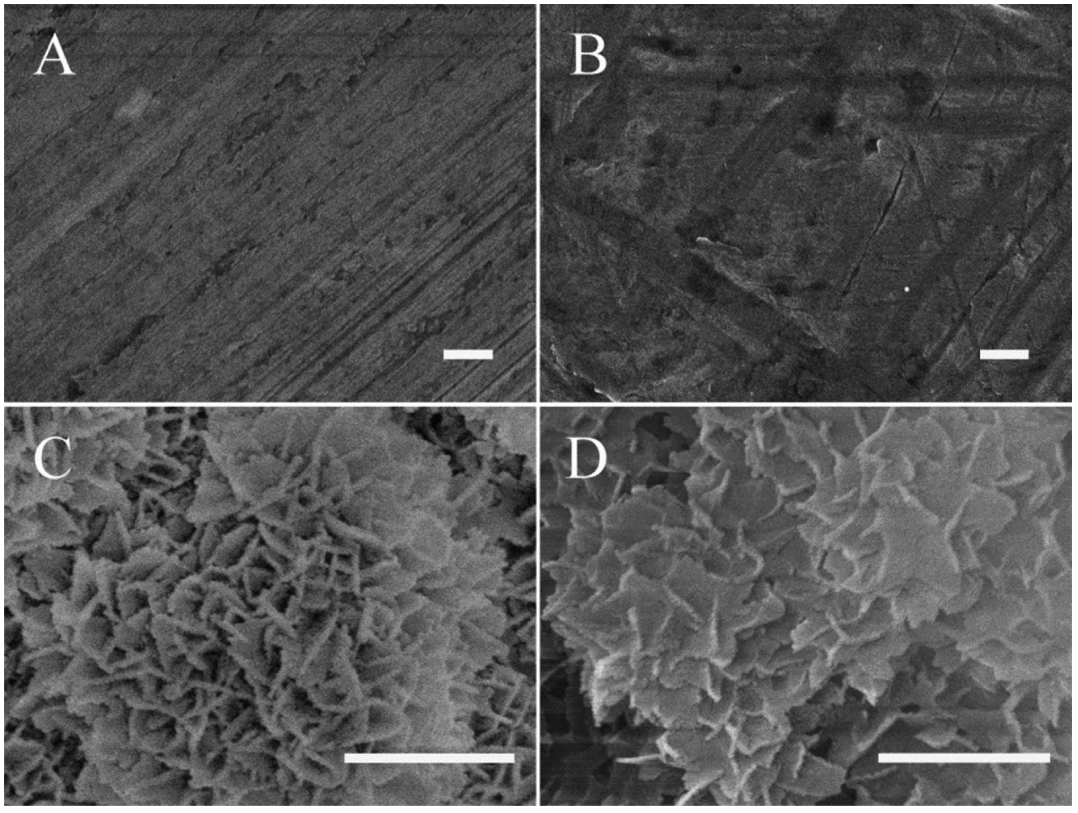

Figure 2. SEM images of samples (A) smooth aluminum 1#, (B) PTES-coated smooth aluminum 2#, (C) etched aluminum 3#, and (D) etched aluminum with PTES coating 4#. Scale bars indicate 500 nm.

water (of density, $\rho = 1000\ \mathrm{kg/m^3}$, surface tension, $\sigma = 0.0728\ \mathrm{N/m}$, and viscosity, $\mu = 0.89 \times 10^{-3}\ \mathrm{Ns/m^2}$) was cooled with a thermostatic bath as the source of overcooled water. During the impact experiment, air was pumped by the dispensing system to release overcooled water droplets (10 μL) from the needle. The whole set up was enclosed in a temperature environmental chamber (DIS-GDS, China) with a controlled temperature and RH. The impact dynamics of a droplet was recorded using a high speed camera (Phantom v710, USA) operated with a frame speed of 3000 frames per second (fps) and an image resolution of 1024 × 768 pixels. A cold lighting system (CEL-S500/350, Aulight, China) was used to backlight the impacting droplet on the target surface.

Several parameters would influence the droplet impact dynamics, such as droplet size, liquid surface tension and impact velocity (v_i). These effects were described in terms of a dimensionless number, the Weber number (W_e) defined by eq 1.

$$W_e = \frac{\rho R v_i^2}{\sigma} \tag{1}$$

Here R is the radius of the liquid droplet (calculated from the droplet volume), v_i is the average impact velocity (was the result of the impact height divided by the whole dropping time), ρ is the liquid density, and σ is the surface tension.

Ice adhesion tensile strength tests were performed using INSTRON 3366 universal testing machine (Instron Corp., USA) in an air-conditioned chamber with a method described in our previous work.[25] In the test, the up and low patterns were made of bare aluminum plate, and the sample was stuck to the low pattern using glue. The interspace between the up and low patterns was fully filled with deionized water. After the assembly of the pattern pairs was placed in a freezer at −10 °C for 24 h, the tensile strength of the ice adhesion was tested in the air-conditioned chamber at −10 °C with the tensile speed of 0.5 mm/min. The multiple ice-breaking tests were conducted by repeating this process for 20 cycles. Meanwhile, multiple ice-melting tests were performed by preparing the samples in the same way as the ice adhesion strength tests. Then the frozen pattern pairs were placed in room temperature to allow the ice between up and low patterns to melt. The ice adhesion strength of this sample was tested in every 5 icing/ice-melting cycles. Each sample for ice-breaking and ice-melting was cleaned with ultrapure water and dried at 100 °C for 4h before next testing cycle.

RESULTS AND DISCUSSION

Surface Morphology and Wettability under Different Temperature and Humidity. *Surface Morphology.* The

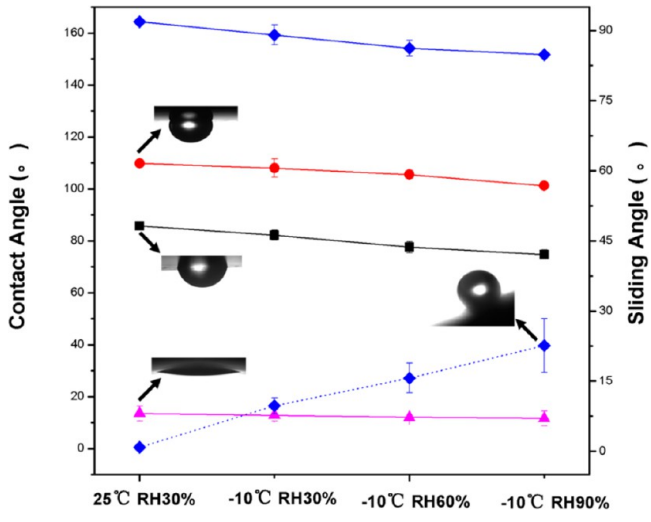

Figure 3. Water CA and SA on four samples at 25 °C with RH 30%, and at −10 °C with RH of 30, 60, and 90%: CA of 1# (solid black line), 2# (solid red line), 3# (solid magenta line), 4# (solid blue line), and SA of 4# (dashed blue line).

dx.doi.org/10.1021/am400429q | ACS Appl. Mater. Interfaces 2013, 5, 3370−3381

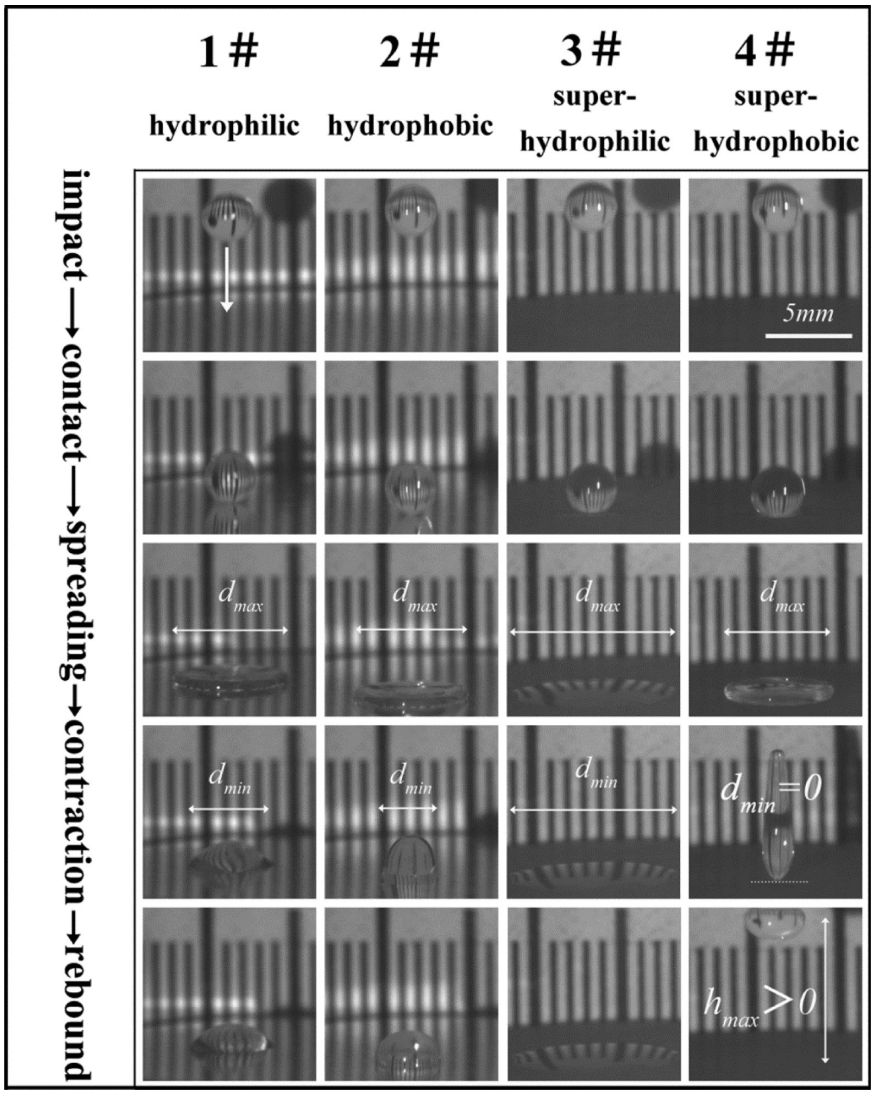

Figure 4. Sequential images of the dynamic behavior of ~10 μL droplets impacting horizontal surfaces from a 5 cm height at −10 °C under RH of 45−55%. Images from top to bottom depict the droplet at impact, contact, maximum spreading (d_{max}) and maximum retraction (d_{min}), and maximum rebound (h_{max}). Droplets were observed to stick on the hydrophilic (1#), hydrophobic (2#), and superhydrophilic (3#) surfaces, whereas they fully retract and rebound on the superhydrophobic surface (4#).

Figure 5. Schematic diagram of an impact cycle of an overcooled water droplet at different stages: impact, contact, spreading, contraction, and rebound.

surface morphologies of the 4 samples were checked by SEM. As shown in Figure 2, the as-received aluminum surface (Sample 1#, Figure 2A) was relatively smooth despite some submicrometer scratchlike defects, which occupied less than 5% of the whole area. PTES coating on this surface only filled some of the very tiny scratches, but no apparent change could be seen to the large defects in the topography (Sample 2#, Figure 2B). After the aluminum surface was etchedby the mixed acid solution for 40s, the surface was fully covered with micro spheres which were densely assembled with nanopetals (Sample 3#, Figure 2C). This binary nano/microstructure was formed by selective etching of vulnerable dislocation inside the Al crystals.[22] It should be noted that some difference in the topography of the etched samples was observed based on brand and batch diversity. Figure 2D presents the surface structure of the PTES-coated surface of this etched sample (Sample 4#). It is noted that as PTES coating covered some subtle nanostructures, the image of the petal-assembled spheres became a little fuzzy compared with the sample before coating (Figure 2C).

Wettability under Different Temperature and Humidity. These four surfaces (Figure 2) are expected to have different wettability from superhydrophilic (Sample 3#), hydrophilic (Sample 1#), hydrophobic (Sample 2#) to superhydrophobic (Sample 4#). Their water CA and SA measurements under an indoor environment (25 °C, RH = 30%) and at −10 °C with different humidity (RH=30, 60, 90%) (Figure 3) showed that

dx.doi.org/10.1021/am400429q | ACS Appl. Mater. Interfaces 2013, 5, 3370−3381

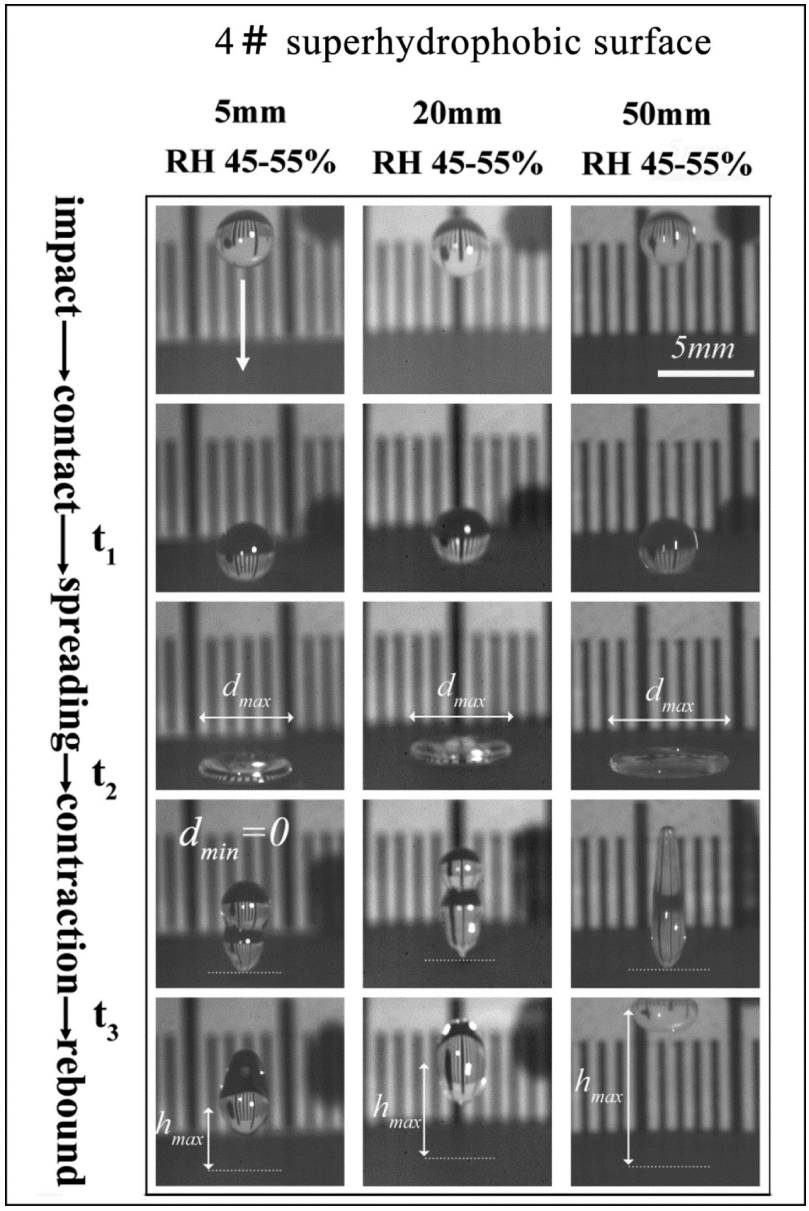

Figure 6. Sequential images of the dynamic behavior of 10 μL of overcooled water droplet impact a horizontal superhydrophobic surface from a height of 5, 20, and 50 mm at −10 °C under RH of 45−55%: Images from top to bottom depict droplet at impact, contact, maximum spreading (d_{max}), maximum retraction (d_{min}), and maximum rebound (h_{max}). Scale bars indicate 5 mm.

they indeed had the wettability as expected. A water droplet spread extensively on Sample 3# with a CA less than 15°, whereas this value increased to 86, 125, and 164° for Samples 1#, 2#, and 4#, respectively. Water droplets can hang upside down on the surfaces of Sample 1#, 2#, and 3#, indicating strong surface adhesion, thus droplet could not slide on these three surfaces. In the meantime, Sample 4# obtained excellent sliding ability with CA of 164.4 ± 0.9°, and SA of 0.84 ± 0.19° at 25 °C and RH 30%. However, the CA decrease and SA increase markedly to 159° and 9.7° when the temperature reduced to −10 °C under the same RH, and they almost linearly changed to 154 and 152°, and 15.7 and 22.6°, with the RH increased to 60 and 90%, respectively.[24,26−28] This trend on the superhydrophobic surface was similar with that on lotus leave,[9] where with the RH changed from 10% to 90% at −10 °C, CA and SA changed from 163 and 6° to 138 and 20°. This change must be associated with water condensation inside the micro/nanostructure of the superhydrophobic surface under the condensing condition with a low temperature and a high RH.[9] Thermodynamically, due to the extremely low surface tension, water condensation in the micro/nanostructure of a superhydrophobic surface only occurred at an oversaturated condition.[29] In the present experiments, the temperature of the atmosphere in the chamber, the dropping water and the testing sample, and the RH of the atmosphere were carefully controlled at −10 °C and 90%. Therefore, the oversaturated condition to condense moisture from atmosphere was not reached under this experimental condition. However, because of the fluctuation of the temperature and humidity in the chamber, especially when water droplets were approaching the surface to create a nearly saturated environment around the sample, in addition with a certain heterogeneity in chemical composition of the superhydrophobic surface, local oversaturation in a small area inside the micro/nanostructure of the superhydrophobic surface could be possible.[29] This would result

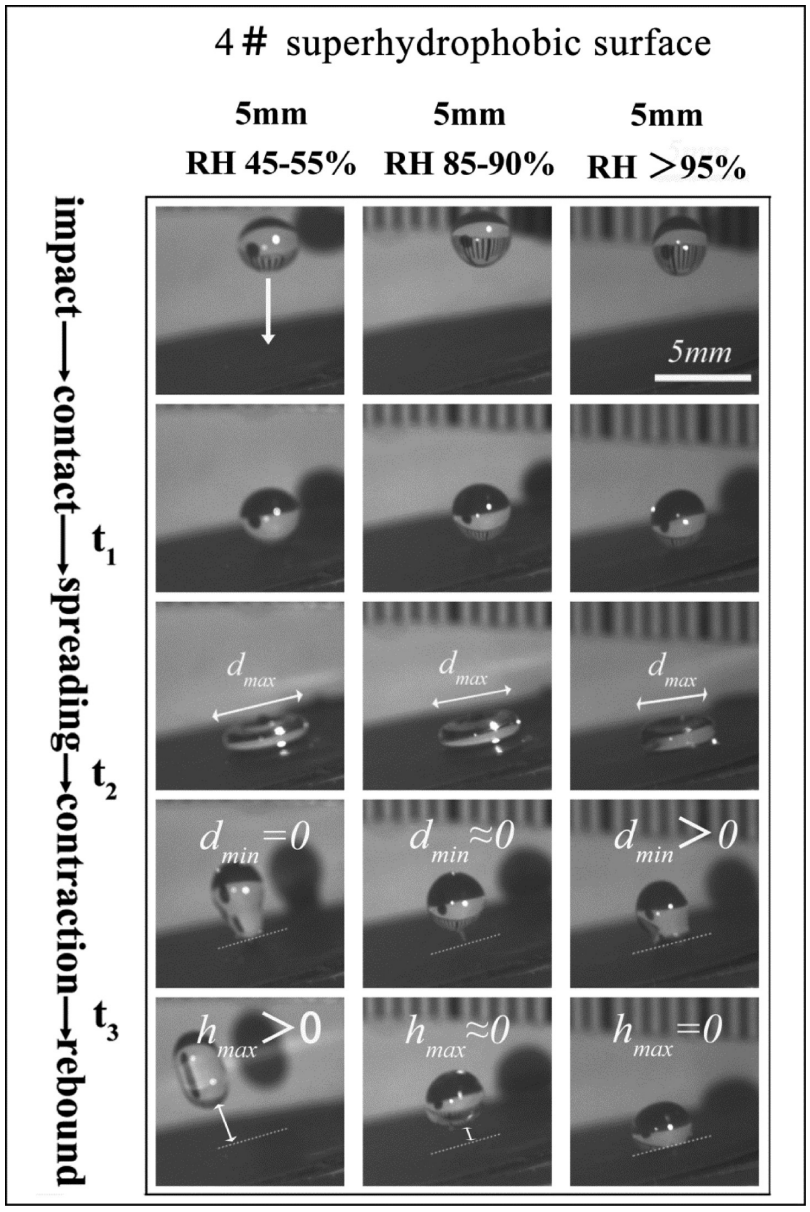

Figure 7. Sequential images of the dynamic behavior of 10 μL overcooled water droplet impact a 10° inclined superhydrophobic surface from 5 mm height at −10 °C under RH of 45−55%, 85−90%, and >95%: Images from top to bottom depict the droplet at impact, contact, maximum spreading (d_{max}), maximum retraction (d_{min}), and maximum rebound (h_{max}). Scale bars indicate 5 mm.

Table 1. Dynamics Data Extracted from Figures 6 and 7 for the Impact on the Superhydrophobic Surface at a Title Angle (TA) of 0 and 10°, Respectively

TA (deg)	H (mm)	RH (%)	v_i (m/s)[a]	W_e[a]	d_{max}(mm)	d_{min}(mm)	h_{max}(mm)	v_1(m/s)	v_2(m/s)	v_3(m/s)[b]
0	5	45−55	0.31	0.80	4.92	0.00	3.75	1.14	0.38	0.26
0	20	45−55	0.63	7.18	5.11	0.00	6.58	1.39	0.38	0.32
0	50	45−55	0.99	17.96	6.16	0.00	9.24	1.76	0.51	0.30
10	5	45−55	0.31	0.80	4.21	0.00	3.94	0.87	0.35	0.35
10	5	85−90	0.31	0.80	4.39	0.00	2.50	0.88	0.28	1.10
10	5	>95	0.31	0.80	4.13	2.07	0.00	0.78	0.16	0.00

[a]See eq 1 for the definition. [b]The error for the v_3 measurement under the high RH is large because of the high energy dissipation, which leads to an incomplete rebound of the droplet.

in local condensation inside the micro/nanostructure, and lead to a lower CA and higher SA value at a high RH. Only under a fully oversaturated condition would the water vapor from environment heavily condense inside the micro/nanostructure of a superhydrophobic surface, and the condensed water would take place the air cushion.[9] Consequently, the droplet wetting model could change from Cassie−Baxter state[30] to Wenzel state[31] and surface adhesion became stronger because of higher

dx.doi.org/10.1021/am400429q | ACS Appl. Mater. Interfaces 2013, 5, 3370−3381

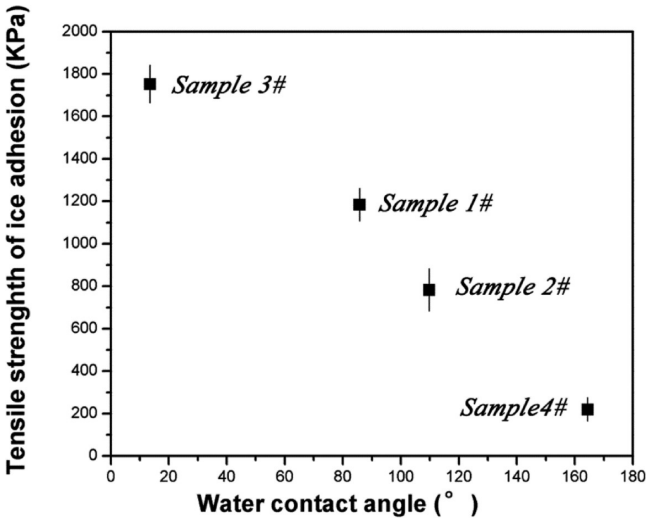

Figure 8. Tensile strength of ice adhesion on four samples: the relationship between ice adhesion and water contact angle.

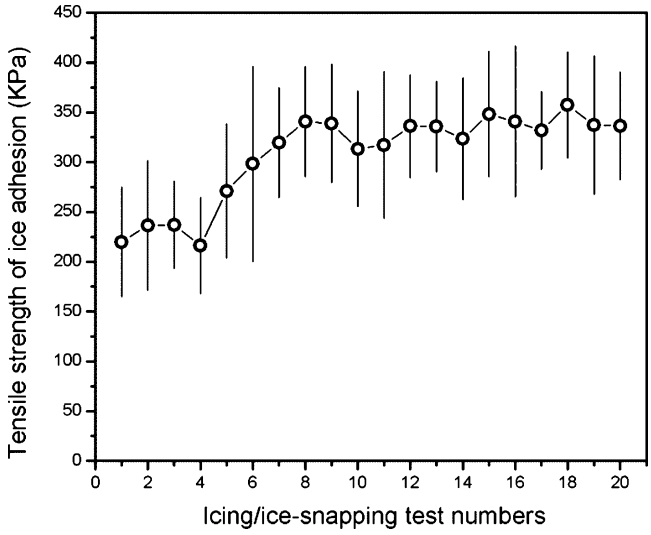

Figure 10. Tensile strength of ice adhesion on 4# superhydrophobic surface in 20 icing/ice-breaking cycles.

solid−liquid interaction.[32] Fortunately, this is not the case for our superhydrophobic sample (Sample 4#), where only local oversaturation under a condensing condition (−10 °C, RH 90%) was observed to increase SA to 22.6 ± 5.77°, corresponding to lotus leaf at the same condition with the sliding ability survived. This ability under the condensing condition plays a critical role to an active anti-icing surface.[7,12,33]

Impact Dynamics of Overcooled Water Droplets. *On Substrates with Different Wettability.* Figure 4 displayed the impact behavior of overcooled water droplets (10 μL) on these four substrates at −10 °C and RH 50 ± 5% with 50 mm releasing height. A high-speed video camera was used to capture sequential images of the droplet at impact, contact, maximum spreading, maximum retraction, and rebound (if occurred).[7] The respective diameters of the droplet at maximum spreading (d_{max}) and maximum retraction (d_{min}), and the rebounded height (h_{max}) were recorded. A small impact height (50 mm) was used in this test in order to reduce energy disturbing,[34] and thus the droplet impact on the surface only in a low Weber number ($v_i \approx 0.99$ m/s, $w_e \approx 17.96$). The water droplet underwent significant retraction on the hydrophilic (1#) and hydrophobic surface (2#), but they remained pinned and did not fully withdraw from the surface, followed by several slight horizontal vibration until the energy depleted, where $d_{max} > d_{min} > 0$. There is no rebounding found on both surfaces except the droplet on Sample 2# had a smaller d_{min}, indicating a more hydrophobic state than Sample 1#. The overcooled water droplet spread on the superhydrophilic surface (3#), but with a negligible retraction, i.e., $d_{max} \approx d_{min}$. Though the droplet on the superhydrophobic surface (4#) spread to a similar d_{max} as on 1# and 2#, it rebound after complete retraction, to a height of 9.24 mm, about 18% of the impact height. It rolled off the superhydrophobic surface after four rebounds.

When an overcooled water droplet was released to a solid surface, the kinetic energy of the droplet dissipated during the spreading process due to impacting, overcoming resistance from viscosity, converting to surface energy and so on. If the energy dissipation (mostly determined by the surface properties) during spreading was not too large, part of surface energy could revert to

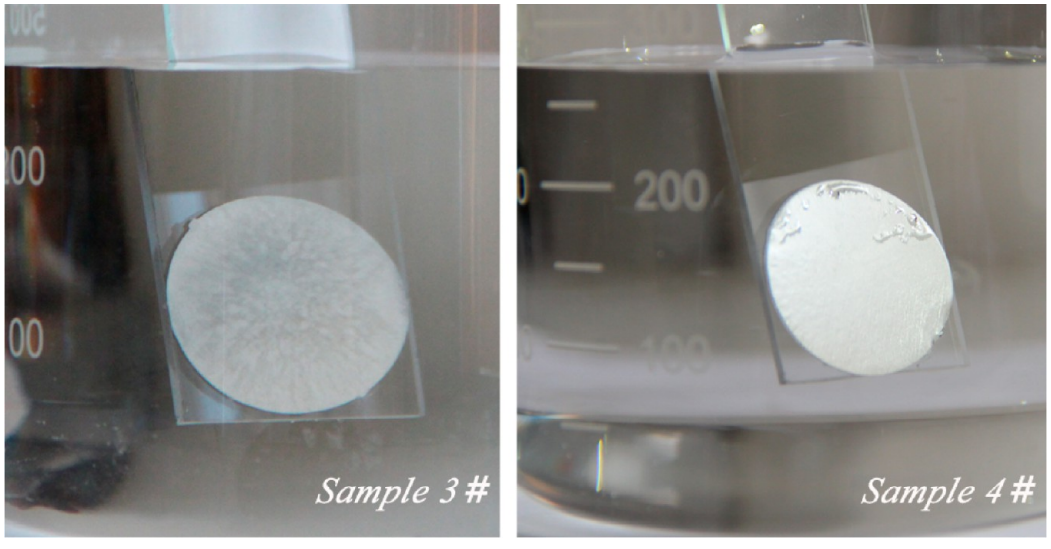

Figure 9. Air trapped between solid and liquid could be seen through the mirror phenomenon.

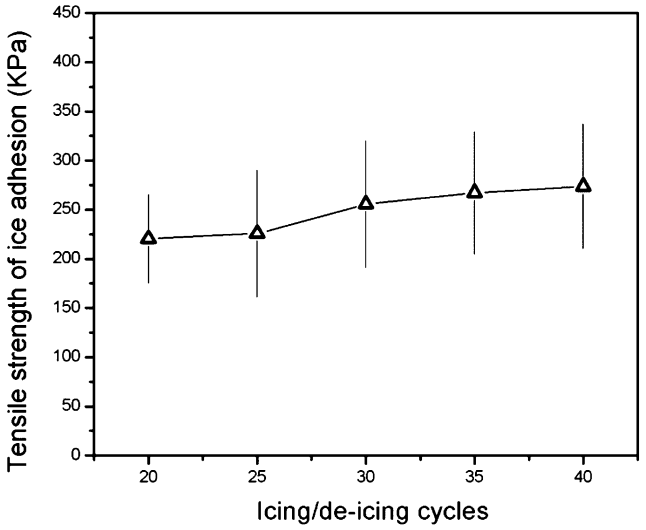

Figure 11. Tensile strength of ice adhesion on 4# superhydrophobic surface after 40 icing/ice-melting cycles.

Table 2. CA and SA from Wettability Test, and Average Height (h) and Mean Deviation (R_a) from AFM Test of Sample 4#, before and after Multiple Icing/Deicing Cycles

samples	CA (deg)	SA (deg)	h (μm)	R_a (μm)
4#	164.4 ± 0.9	0.84 ± 0.19	4.575	1.250
20 ice-breaking	150.6 ± 0.3	51.4 ± 3.9	4.046	0.986
40 ice-melting	154.1 ± 0.4	44.3 ± 3.2	3.479	0.727

the kinetic energy and lead to retracting and rebounding.[12] Otherwise, the droplet remained pinned on the surface instead of fully withdraw and rebound before energy was expended. On the other hand, ice formation speed of an overcooled water droplet on solid surface depended on the growth rate of crystal nucleus. The ice formation of an overcooled water droplet on subzero surface could be delayed but could not be fully prevented. Mishchenko et al.[7,13] showed that water droplets impinging on superhydrophobic surfaces exhibited a nonicing behavior if the time scale for droplet spreading and retracting from the surface was smaller than the ice nucleation time, and the droplet would bounce or roll off the surface before ice nucleating. During a droplet fell, its kinetic energy of droplet was only related to the releasing height, but not the surface properties. However, the kinetic energy and surface properties both contributed to the spreading for the droplet to reach d_{max}.[33,35] This impact dynamics study indicated that kinetic energy loss dominated this process as d_{max} was almost the same on the hydrophilic, hydrophobic and superhydrophobic surfaces. The retraction process where the droplet diameter changed from d_{max} to d_{min} could mainly reflect the interaction between water droplet and surface. Since the lowest interaction and adhesion between solid−liquid on the superhydrophobic surface, the energy dissipation during spreading and retraction is less than that on other three surfaces. Therefore, the spread water droplet can retract to a state similar to a static contact droplet at the Cassie−Baxter wetting model, and rebound off easily on the superhydrophobic surface before it froze.

On the Superhydrophobic Surface with Different Releasing Height and Humidity. A complete droplet impact cycle from impact to rebound only occurred on the superhydrophobic surface. With the help of high-speed photography analysis, we can define the time of each stage of a whole cycle as

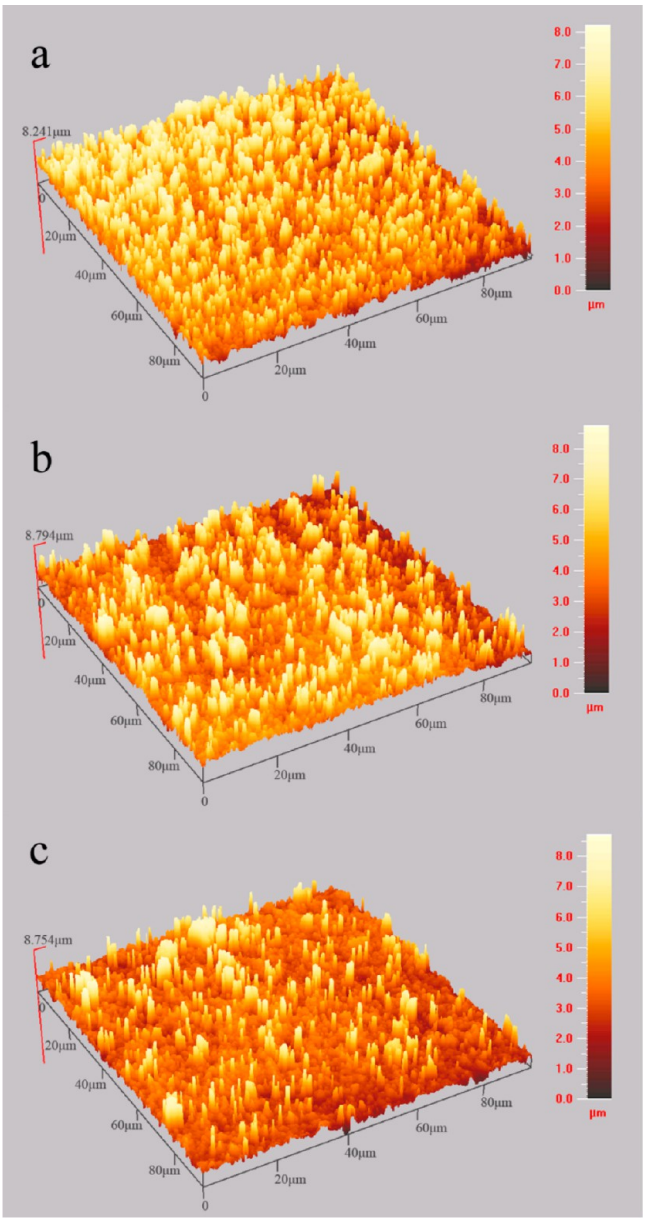

Figure 12. Three-dimensional surface profile of the superhydrophobic surface (Sample 4#), (a) before and (b, c) after (b) 20 icing/ice-breaking and (c) 40 icing/ice melting cycles.

demonstrated in Figure 5, where t_1 is the time from contact to maximum spreading (d_{max}), then t_2 to complete contracting (d_{min}, which is 0 for Sample 4#), and t_3 to maximum rebounding (h_{max}). Accordingly, the mean velocity for water spreading, contracting and rebounding in these periods was v_1, v_2, and v_3, respectively, $v_1 = (d_{max})/(t_1)$, $v_2 = (d_{max} - d_{min})/(t_2)$, $v_3 = (h_{max})/(t_3)$.

Figure 6 and Figure 7 displayed the first impact cycle of a 10 μL overcooled water droplet impacted on horizontal and tilted (10°) superhydrophobic surfaces with different releasing height and humidity. Figure 6 focused on the effect of the releasing height on the impact dynamics under a low humidity (50 ± 5%). Figure 7 described the impact process on a tilted (10°) superhydrophobic surface under different humidity levels of 50, 90, and 95% to mimic different weather conditions. The data extracted from Figures 6 and 7 are summarized in Table 1.

Table 1 indicated that in the spreading period, d_{max} and v_1 displayed a positive correlation with the increase of releasing

dx.doi.org/10.1021/am400429q | ACS Appl. Mater. Interfaces 2013, 5, 3370−3381

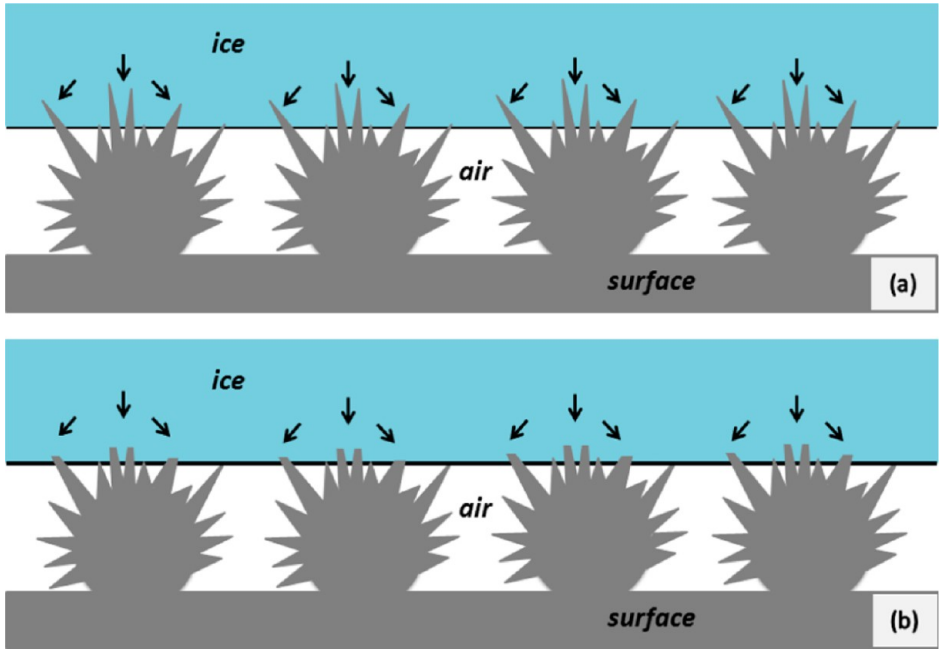

Figure 13. Schematic illustration of (a) the surface structure with ice, and (b) its damage caused by the icing/deicing processes.

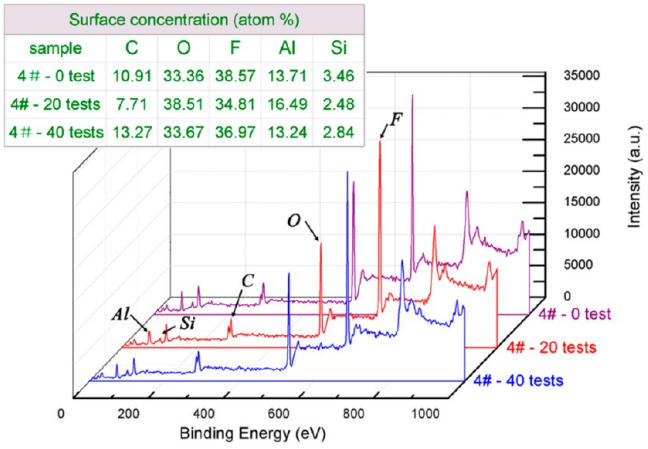

Figure 14. XPS spectra of the superhydrophobic surface (4#, 0 test), and after 20 cycles of ice-breading test (20 tests) and 40 ice-melting tests (40 tests). The inset table shows surface elemental concentrations of the three samples.

height under a fixed humidity (50%). However, d_{max} and v_1 remained almost constant with the increase in humidity at the same releasing height (5 mm), indicating that kinetic energy loss dominated the movement of the droplet while the influence of surface properties was negligible. The retraction period where the droplet retracted from d_{max} to d_{min} could mainly reflect the interaction between the droplet and surface. In this period, v_2 remained unchanged at the releasing height of 5 and 20 mm, but significantly decreased with the increase of humidity, suggesting that droplet had a higher adhesion with the surface at a high humidity. Moreover, the rebound height (h_{max}) dramatically dropped with the increase of humidity. A droplet could not rebound on the superhydrophobic surface under RH > 95%, indicating the kinetic energy was not high enough to conquer the surface adhesion at RH > 95%. Both the v_2 and h_{max} results suggest that the superhydrophobic surface has an increased water adhesion with the increase of humidity. The v_3 data under high humidity showed a poor consistence. It is believed that this is caused by a large error in the rebounding height (h_{max}) measurement. Because of the high energy dissipation under the high humidity, the droplet rebound was incomplete to cause a large deformation of the droplet. This could lead to a large error in the h_{max} measurement.[36]

On Large Superhydrophobic Surfaces with Different Tilt Angle and Humidity. In above experiment, the surface is only 26 mm in diameter, which is too small to investigate the whole rebounding process of droplets on the surface. In order to have a more comprehensive study, larger (75 × 25 mm^2) superhydrophobic samples were prepared and investigated fot the impact of single and successive water droplets at −10 °C with different tilt angle and humidity.

Our results suggested that the rebounding behavior was significantly depended on the tilt angle and humidity. A single droplet released from 5 mm to the superhydrophobic surface tilted at 10° would rebound four times in average and then roll off the surface under a low humidity (RH = 50 ± 5%). However, a water droplet would rebound only twice and then adhere to this surface when the humidity was increased to RH 85−90% (see movie 1 in the Supporting Information). But it could still roll off the surface after one rebound if the tilt angle increased to 30° (see movies 2 in the Supporting Information).

The impact dynamics of successive water droplets on the superhydrophobic surface was also investigated by releasing 10 droplets of the overcooled water from 5 mm height at a speed of 3 droplets per second to a same spot of the surface under the same condition as the single droplet test (see movie 3 in the Supporting Information). It was observed that their behavior was similar to the single droplet, ie. under a low humidity (RH = 45−55%), all the droplets rolled off the surface after several rebounds at 10° of the tilt angle, while under a high humidity (RH = 85−90%), they rebound once and then only could roll off when the tilt angle larger than 30°. Variation in the rolling process was observed for different droplets, some droplets rolled off the surface directly, while some others would stay on the surface after rolling a certain distance and merged with succeeding droplets

into a bigger one and then rolled off the surface. Therefore, we can reasonably conclude that water droplets could roll off the surface as long as surface tilt angle is greater than 30° under this high condensing condition with −10 °C and RH 85−90%.

Ice Adhesion on Superhydrophobic Surfaces. *On Surfaces with Different Wettability.* Now, it is clear that a superhydrophobic surface could let overcooled water droplets rebound or roll off under a relative low humidity to serve as a good icephobic surface.[7] However, it only allowed the overcooled water droplets to slide off the surface with a tilt angle larger than30° under a highly condensing condition of −10 °C and RH 85−90%. In other words, under this highly condensing condition, water or ice would accumulate on the surface with a tilt angle less than 30°. Unfortunately, this type of weather was frequently encountered in winter of the cold area in the world such as during heavy freezing rain and wet snow, where ice would eventually accumulated on the surface of many objects. In this case, the adhesion of the ice with the surface play a critical role for an icephobic or anti-ice surface,[8] where the adhesion is expected to be as weak as possible. In this work, we have tested the tensile adhesion strength of ice on these 4 surfaces with the results illustrated in Figure 8. A good correlation between CA and ice repellency could be seen from this figure. The ice adhesion increased with the decrease of the surface CA. The tensile adhesion strength significantly decreased from 1700, 1200, 800, to 200 KPa when the surface change from superhydrophilic (3#), hydrophilic (1#), hydrophobic (2#), and superhydrophobic (4#). Though the superhydrophilic surface and superhydrophobic surface both have a similar binary nano/microstructure formed in the etching process, the ice adhesion strength on the superhydrophilic surface was about 8 times higher than that on the superhydrophobic surface. This difference must be attributed to the surface wettability. The superhydrophilic surface of the etched aluminum plate was converted to the superhydrophobic by coating a cross-linked PFES layer on the surface. This surface property change not only changed the water contact angle from less than 15 to 164°, but also the icing behavior. Water on the superhydrophilic surface would easily penetrate into the cavities of the nano/microstructure and then froze to form a root-like structure to anchor the ice layer into the nano/microstructure on the surface to promote the ice adhesion. On the contrast, the water-repellent property of the superhydrophobic surface would maintain air trapped inside the cavities of the nano/microstructure in great extent even under a condensing weather condition as discussed previously, and thus an "air cushion" would remained between the water and solid surface, after water froze, the air cushion would significantly reduce the contact of the ice with the substrate and hence greatly reduced the ice adhesion strength.

The existence of "air cushion" was demonstrated by a simple and intuitive immersing experiment,[37] where both Sample 3# and Sample 4# were immersed into water and viewed at different angles as shown in Figure 9. It is found that Sample 3# showed a normal Al color, indicating a completely wetted surface, while Sample 4# appeared as a silver mirror when viewed at a glancing angle, which was about 50°, where the light was reflected at the water/air interface to display a shining color. This mirrorlike appearance was maintained even after the sample was immersed in water at 0 °C for 1 h. This appearance indicates the "air cushion" can stably stay between the superhydrophobic surface and water, even in freezing water.

Durability of the Icephobic Performance of the Superhydrophobic Surface. It can be seen from above discussion that the superhydrophobic surface of Sample 4# can be served as an icephobic surface since overcooled water droplets rebound and roll off the surface rapidly as well as ice adhesion on the surface is significantly reduced. However, for the real application, a high durability of this property is important as well.[6,8,14,38]

Therefore the durability of icephobic performance on this superhydrophobic surface was investigated by applying multiple icing/ice breaking and icing/ice melting cycles to the surface.

The ice adhesion of Sample 4# were measured over 20 icing/ice-breaking cycles, and the result was shown in Figure 10. It showed that the ice adhesion was increased about 50% from 220 KPa to 340 KPa in the initial 8 cycles and then leveled off until 20 cycles. The final adhesion was still much lower than any other samples in this work, only 20% of the strength on the superhydrophilic surface (3#), suggesting the anti-ice properties of this surface could survive from the multiple ice-breaking processes. In addition, Figure 11 indicated that ice-melting tested sample had an even much milder increase of the ice adhesion, increased from 220 KPa to 272 KPa, less than 25% increase over 40 icing/ice-melting cycles. This might indicate that the ice-melting process created a less damage to the superhydrophobic surface structure. The results from the both tests demonstrated an excellent durability of the icephobic property of our superhydrophobic surface. This durability is better than the superhydrophobic surface prepared using a similar way reported previously.[6] We believe this difference is attributed to the difference in the toughness of the surface nano/microstructure prepared by acid etching. It should be noted a different etching solution and shorter etching time was used in our work.

To verify this assumption, the superhydrophobic surfaces after the ice-breaking and ice-melting test were further investigated regarding their wettability and surface topological and chemical structures and compared with the sample before these tests. Therefore, the CA, SA, surface profile and XPS tests were conducted to the original Sample 4#, the samples after 20 icing/ice-breaking cycles and 40 icing/ice-melting cycles.

The CA and SA measurements of the three samples were taken under an indoor environment (25 °C, RH = 30%) and the results were listed in Table 2. It showed that both 20 icing/ice-breaking sample and 40 icing/ice-melting samples lost part of their hydrophobicity with CA decreased from 164 to 150 and 154°, and SA increased from 0.84 to 51.4 and 44.3° for the ice-breaking and ice-melting samples, respectively. It showed that the loss of the ice-breaking sample was slightly significant than the ice-melting sample. This trend coincided with the loss of icephobic property.

The three-dimension surface morphology of these three samples was shown in Figure 12. Average height (h) and mean deviation (R_a) of each sample was measured from these profiles with the result listed in Table 2. Figure 12 showed that the density of the surface sharp-structure decreased after the multiple ice-breaking and ice-melting processes, leading to an apparent decrease of the average height of the microspheres assembled with the nanopetals as depicted in Figure 13. However, the micronano hierarchical structure still partially survived. Meanwhile, Figure 12 also showed that the ice-melting sample showed a heavier damage to the micro/nanohierarchical structure than the ice-breaking sample in terms of the loss of petal structure and the decrease in the average height. By considering that the ice-melting sample had suffered 20 more freezing cycles than the ice-breaking sample, we believed that the water freezing process would produce more pronounced damage to the hierarchical structure than the ice breaking process. It is reported that the

fracture stress in a capillary-porous system could be varied between 5×10^4 and 2×10^8 Pa,[39] which was high enough to break the hierarchical structure in the superhydrophobic surface. However, this result is not consistent with that from the ice adhesion test and the surface wettability test described above, which indicated a slight more damage of the ice-breaking process than the ice-melting process. To explain this contradiction, we investigated the surface chemical composition of these three samples and compared them using XPS.

Figure 14 displays the XPS spectra of the original Sample 4# and the samples after 20 icing/ice-breaking and 40 icing/ice-melting cycles. In the XPS analysis, 5 random spots were tested on each sample and the reported data were the average of these five tests. It showed that the samples after these multiple deicing processes had a reduced F, Si and O concentration, indicating a light deterioration of the PTES surface coating. Furthermore, comparing to the ice-melting sample, the ice-breaking sample had even lower F, Si and O concentrations on the surface. This result suggested that the ice-breaking process created more damage to the hydrophobic coating than the ice-melting process. This explained the fact that the ice-breaking process generated larger lose in the icephobic properties of the superhydrophobic surface. Therefore, though both of the binary nano/micro-hierarchical structure and the low surface tension are equally important to superhydrophobic as well as icephobic property, as long as the hierarchical structure is dense enough to support the water droplet to form an air cushion between the substrate and surface, the effect due to the partially loss of the hierarchical structure is less pronounced than the loss of the surface hydrophobic coating layer. This result will provide us a trend in designing durable icephobic surfaces.

CONCLUSION

Four surfaces with superhydrophilic, hydrophilic, hydrophobic, and superhydrophobic properties were prepared with aluminum plate. The superhydrophilic surface was obtained by etching the aluminum surface with an acid, and the superhydrophilic surface was converted to the superhydrophobic surface by coating a PTES layer using a simple dip coating process. The SA of this superhydrophobic surface at 25 °C and RH 30% was very low, only 1°. This value increased to 22° under an extremely condensing condition (−10 °C, RH 90%), where both single and successive overcooled water droplets could rebound on the surface and roll off the surface at a tile angle larger than 30°. This result indicated that droplets of overcooled water were able to roll off the surface before froze even under this extreme condition, meaning an active ice-repellent surface could be realized.

Furthermore, the ice adhesion on this superhydrophobic surface was significantly reduced, only 13% of that on the superhydrophilic surface. This feature was owed to the formation of an "air cushion" between the surface and water. This feature also reduceed damage to the superhydrophobic structure upon deicing processes, and offered the surface a better durability of the icephobic performance. After 20 icing/ice breaking cycles and 40 icing/ice-melting cycles, the ice adhesion strength of the surface only slightly increased from 13 to 20 and 16% comparing to the superhydrophilic surface, respectively, demonstrating an excellent durability as an active icephobic surface. Surface profile and XPS study indicated that this durability was associated with a relative strong micro/nanosurface structure and a tough PTES coating.

ASSOCIATED CONTENT

Supporting Information

Supplemental movies on the impact of overcooled water droplets on large superhydrophobic surfaces with different tilt angle and humidity (.avi). This material is available free of charge via the Internet at http://pubs.acs.org.

AUTHOR INFORMATION

Corresponding Author

*Tel.: 86-25-83593289. Fax: 86-25-83593048. E-mail: chenqm@nju.edu.cn.

Notes

The authors declare no competing financial interest.

ACKNOWLEDGMENTS

The authors express thanks to Ms. Zhou for technical assistance with SEM measurement. This work is financially supported by a grant Nanjing University Testing Fund (0205D100).

REFERENCES

(1) Barthlott, W.; Neinhuis, C. *Planta* **1997**, *202*, 1−8.
(2) Guo, Z. G.; Liu, W. M.; Su, B. L. *J. Colloid Interface Sci.* **2011**, *353*, 335−355.
(3) Bhushan, B.; Jung, Y. C. *Prog. Mater. Sci.* **2011**, *56*, 1−108.
(4) Yao, X.; Song, Y. L.; Jiang, L. *Adv. Mater.* **2011**, *23*, 719−734.
(5) Cao, L.; Jones, A. K.; Sikka, V. K.; Wu, J.; Gao, D. *Langmuir* **2009**, *25*, 12444−12448.
(6) Kulinich, S. A.; Farhadi, S.; Nose, K.; Du, X. W. *Langmuir* **2011**, *27*, 25−29.
(7) Mishchenko, L.; Hatton, B.; Bahadur, V.; Taylor, J. A.; Krupenkin, T.; Aizenberg, J. *ACS Nano* **2010**, *4*, 7699−7707.
(8) Kulinich, S. A.; Farzaneh, M. *Appl. Surf. Sci.* **2009**, *255*, 8153−8157.
(9) Yin, L.; Wang, Q. J.; Xue, J. A.; Ding, J. F.; Chen, Q. M. *Chem. Lett.* **2010**, *39*, 816−817.
(10) Xiao, X. C.; Cheng, Y. T.; Sheldon, B. W.; Rankin, J. *J. Mater. Res.* **2008**, *23*, 2174−2178.
(11) Wier, K. A.; McCarthy, T. J. *Langmuir* **2006**, *22*, 2433−2436.
(12) Alizadeh, A.; Yamada, M.; Li, R.; Shang, W.; Otta, S.; Zhong, S.; Ge, L. H.; Dhinojwala, A.; Conway, K. R.; Bahadur, V.; Vinciquerra, A. J.; Stephens, B.; Blohm, M. L. *Langmuir* **2012**, *28*, 3180−3186.
(13) Bahadur, V.; Mishchenko, L.; Hatton, B.; Taylor, J. A.; Aizenberg, J.; Krupenkin, T. *Langmuir* **2011**, *27*, 14143−14150.
(14) Kulinich, S. A.; Farzaneh, M. *Langmuir* **2009**, *25*, 8854−8856.
(15) Sarkar, D. K.; Farzaneh, M. *J. Adhes. Sci. Technol.* **2009**, *23*, 1215−1237.
(16) Tourkine, P.; Le Merrer, M.; Quere, D. *Langmuir* **2009**, *25*, 7214−7216.
(17) He, M.; Wang, J. X.; Li, H. L.; Jin, X. L.; Wang, J. J.; Liu, B. Q.; Song, Y. L. *Soft Matter* **2010**, *6*, 2396−2399.
(18) Dotan, A.; Dodiuk, H.; Laforte, C.; Kenig, S. *J. Adhes. Sci. Technol.* **2009**, *23*, 1907−1915.
(19) Saito, H.; Takai, K.; Yamauchi, G. *Surf. Coatings Int.* **1997**, *80*, 168−&.
(20) Drelich, J.; Chibowski, E.; Meng, D. D.; Terpilowski, K. *Soft Matter* **2011**, *7*, 9804−9828.
(21) Yin, L.; Wang, Y. Y.; Ding, J. F.; Wang, Q. J.; Chen, Q. M. *Appl. Surf. Sci.* **2012**, *258*, 4063−4068.
(22) Qian, B. T.; Shen, Z. Q. *Langmuir* **2005**, *21*, 9007−9009.
(23) Yin, L.; Xia, Q.; Xue, J. A.; Yang, S. Q.; Wang, Q. J.; Chen, Q. M. *Appl. Surf. Sci.* **2010**, *256*, 6764−6769.
(24) Yin, L.; Zhu, L.; Wang, Q.; Ding, J.; Chen, Q. *ACS Appl. Mater. Interfaces* **2011**, *3*, 1254−1260.
(25) Yang, S. Q.; Xia, Q. A.; Zhu, L.; Xue, J. A.; Wang, Q. J.; Chen, Q. M. *Appl. Surf. Sci.* **2011**, *257*, 4956−4962.
(26) Mockenhaupt, B.; Ensikat, H.; Spaeth, M.; Barthlott, W. *Langmuir* **2008**, *24*, 13591−13597.

(27) Karmouch, R.; Ross, G. G. *J. Phys. Chem. C* **2010**, *114*, 4063−4066.
(28) Furuta, T.; Sakai, M.; Isobe, T.; Nakajima, A. *Langmuir* **2010**, *26*, 13305−13309.
(29) Boinovich, L. B.; Emelyanenko, A. M. *Mendeleev Commun.* **2013**, *23*, 3−10.
(30) CASSIE, A. *Discuss. Faraday Soc.* **1948**, *3*, 11−16.
(31) Wenzel, R. N. *Ind. Eng. Chem.* **1936**, *28*, 988−994.
(32) FURMIDGE, C. G. *J. Colloid Sci.* **1962**, *17*, 309−&.
(33) Zheng, L.; Li, Z.; Bourdo, S.; Khedir, K. R.; Asar, M. P.; Ryerson, C. C.; Biris, A. S. *Langmuir* **2011**, *27*, 9936−9943.
(34) Wang, B.; Zhao, Y.; Yu, T. *J. Adhes. Sci. Technol.* **2011**, *25*, 93−108.
(35) Richard, D.; Quere, D. *Europhys. Lett.* **2000**, *50*, 769−775.
(36) Kannan, R.; Vaikuntanathan, V.; Sivakumar, D. *Colloids Surf., A* **2011**, *386*, 36−44.
(37) Zhu, X. T.; Zhang, Z. Z.; Men, X. H.; Yang, J.; Wang, K.; Xu, X. H.; Zhou, X. Y.; Xue, Q. J. *J. Mater. Chem.* **2011**, *21*, 15793−15797.
(38) Kulinich, S. A.; Farzaneh, M. *Appl. Surf. Sci.* **2009**, *255*, 4056−4060.
(39) Boinovich, L. B.; Emelyanenko, A. M.; Ivanov, V. K.; Pashinin. A. S. *ACS Appl. Mater. Interfaces* **2013**, DOI: 10.1021/am3031272, Just Accepted.